processes

MDPI

Article

Study on the Physicochemical Properties of Biomass-Assisted Enhanced Coal Extraction Process

Yue Kang, Hailan Zhao, Yuanhao Yu and Haibin Zuo *

State Key Laboratory of Advanced Metallurgy, University of Science and Technology Beijing, Beijing 100083, China
* Correspondence: zuohaibin@ustb.edu.cn

Abstract

With the transformation of energy structure to low carbon, the clean and efficient utilization of coal has received extensive attention. Among them, the technology of preparing super-clean coal by solvothermal extraction has become a research hotspot because of its good product characteristics. In this paper, FGZ coal was used as a raw material to explore its synergistic extraction effect with wood charcoal at different mass ratios, and the extracted products were systematically characterized by various analytical methods. The results show that the addition of biomass can effectively improve the extraction yield of this coal. When the biomass addition ratio was 35%, the extraction yield reached the highest value of 69.47%, which was about 28.3% higher than that without biomass. Hypercoal has a smooth surface with significantly fewer impurities than raw coal. At the same time, Raman spectroscopy and X-ray diffraction analysis showed that when the biomass addition ratio was 35%, the I_D/I_G reached a minimum value of 0.8354, and the structural order of the extracted product was the highest. When the biomass addition ratio was 35%, the L_c reached a maximum value of 2.0569 nm, indicating the highest degree of carbon layer stacking and structural order among the samples.

Keywords: Hypercoal; biomass; extraction; physicochemical properties; mechanism

1. Introduction

With the global energy structure undergoing low-carbon transformation, the efficient and clean utilization of coal has become a crucial component in the energy structure transition, particularly in mitigating environmental issues such as carbon dioxide emissions generated during coal utilization [1,2]. In recent years, the technology of preparing Hypercoal (HPC) via organic solvent thermal extraction has garnered extensive attention owing to its mild reaction conditions, selective cleavage of specific covalent bonds in coal, and maximal retention of aromatic structural units [3–5]. Commonly used organic solvents include N-methyl-2-pyrrolidone (NMP), 1-methylnaphthalene (1-MN), pyridine, 1,2,3,4-tetrahydronaphthalene, etc. [6–8]. The as-prepared HPC possesses advantages of low ash content, high aromaticity, and low impurity content, thereby finding wide applications in metallurgical, chemical, and energy fields [9–11].

Recent studies have demonstrated that adding an appropriate amount of biomass to coal solvothermal extraction can exert a synergistic effect, enhancing extraction yield or improving product performance [12,13]. Shui et al. [14] investigated the co-thermal extraction behavior of Shenhua coal and sawdust, and found that when the thermal extraction temperature ranged from 320 to 340 °C and the coal-to-sawdust mixing ratio

Check for updates

Academic Editors: Hongliang Luo, Yu Jin and Feixiang Chang

Received: 27 December 2025
Revised: 16 January 2026
Accepted: 22 January 2026
Published: 23 January 2026

Copyright: © 2026 by the authors. Licensee MDPI, Basel, Switzerland. This article is an open access article distributed under the terms and conditions of the Creative Commons Attribution (CC BY) license.

was 1:1, the liquefaction conversion rate and oil yield of Shenhua coal increased by 16.8% and 11.4%, respectively. Zhao et al. [12] revealed that in the preparation of HPC from Kelan coal, the addition of 20% Larix principis-rupprechtii sawdust increased the extraction yield and caking index by 16.2% and 12.1%, respectively. The carbon structural order and graphitization degree of coke prepared from this product were significantly improved. Li et al. [13] showed that the soluble components obtained by co-extraction of lignite and straw could serve as low-cost carbon fiber precursors; the resulting carbon fibers exhibited a carbon content exceeding 92% and a diameter of approximately 4–6 μm, which is comparable to that of commercial carbon fibers. Zhao et al. [15] reported that the HPC extraction yields of Xibu coal and Guandi coal increased by approximately 160% and 260% after adding 50% and 20% biomass, respectively. Although the aforementioned studies have confirmed the synergistic effect between coal and biomass, most current research focuses on a limited number of specific coal types. As an important coal resource in China, Fangezhuang (FGZ) coal (a type of Chinese fat coal) features unique coal petrographic composition, molecular structure, and mineral occurrence characteristics [16]. However, research on the preparation of HPC via synergistic biomass extraction from FGZ coal remains scarce.

Beyond its synergistic role in ultra-clean coal extraction, biomass has attracted considerable interest in various metallurgical and energy-related processes due to its renewable nature [17–19]. For example, raw woody cellulose has been utilized in iron ore reduction, producing metallic iron while concomitantly reducing carbon dioxide emissions [20]. Reduction products obtained using biomass as a reducing agent exhibit the advantage of low ash content [21]. In mineral processing, the use of biomass as a reducing agent enables the reduction of low-grade iron ore to improve its quality while lowering energy input [22]. Additionally, scholars have explored innovative methods for selectively separating manganese and iron from complex ores using biomass such as horse manure, leveraging organic acids produced during biomass decomposition to achieve efficient metal recovery [23,24]. These studies indicate that biomass is increasingly functioning not only as a supplementary fuel or reducing agent but also as an active reagent in material conversion and separation technologies.

In this study, FGZ coal was selected as the research object to investigate its synergistic extraction behavior with biomass at different mass ratios. The coals before and after extraction were characterized using X-ray diffraction (XRD), X-ray photoelectron spectroscopy (XPS), Fourier transform infrared spectroscopy (FTIR), Raman spectroscopy (Raman) and scanning electron microscopy (SEM). The objectives were to clarify the effects of biomass addition on the extraction yield, as well as the composition and structure of FGZ coal-derived products, and further reveal the synergistic mechanism during the co-extraction process. On this basis, the potential application direction of the prepared HPC was further discussed. This study provides a theoretical basis and data support for the efficient, clean conversion and high-value utilization of this kind of coal.

2. Materials and Methods

2.1. Materials

The test coal was collected from FGZ, and the coal sample was dried at 105 °C for 12 h to remove water. After that, it was crushed to pass through the 200-mesh standard square hole sieve and mixed. Biomass used was wood charcoal, and NMP (Beijing InnoChem Science & Technology Co., Ltd., Beijing, China) was employed as a high-temperature extraction solvent (purity $\geq$ 99.5%). The results of industrial analysis and elemental analysis of coal samples and biomass are shown in Table 1. Proximate analysis (ash, volatiles, fixed carbon) was conducted according to ASTM D3172 [25], respectively, while ultimate analysis

(C, H, N, S, O) was performed in accordance with ASTM D3176 [26] (for CHNS), with oxygen content determined by the differential method.

Table 1. Proximate and ultimate analysis of samples.

	Sample	Proximate Analysis (db, wt.%)			Ultimate Analysis (daf, wt.%)					H/C
		A	V	FC	C	H	O	N	S	
1	FGZ	9.99	27.6	61.54	74.86	4.32	7.79	1.16	0.53	0.69
2	Biomass	16.28	30.11	50.11	58.85	2.88	20.06	1.11	0.00	0.59

A: ash; V: volatile matter; FC: fixed carbon; db: dry basis; daf: dry ash-free.

2.2. HPC Preparation and Evaluation

The experimental vessel was a high-pressure reactor with an effective volume of 5 L (Yantai Songling Chemical Equipment Co., Ltd., Shandong, China). To investigate the synergistic extraction effect of different biomass addition ratios, the solid feedstocks consisted of pulverized coal and biomass mixed at various mass ratios, with a total mass of 30 g. The detailed experimental protocol is presented in Table 2. In accordance with a solid-to-liquid ratio of 1:50 (g/mL), the solid feedstocks were added to the high-pressure reactor together with the NMP solvent. Subsequently, high-purity nitrogen gas was purged at a flow rate of 1.5 L/min for 20 min to remove air from the reactor. Under continuous stirring at 100 rpm, the reaction system was heated to 350 °C and maintained at a constant temperature for 1 h to ensure adequate solid–liquid contact. Upon completion of the reaction, heating was ceased, and the high-pressure reactor was naturally cooled to room temperature before collecting the product mixture. The mixture was separated into a liquid phase and solid residue via vacuum filtration using a Buchner funnel (Sichuan Shubo (GROUP) Co., Ltd., Chongzhou, China). The filtrate was subjected to desolation using a rotary evaporator (Gongyi Yuhua Instrument Co., Ltd., Shanghai, China), and the resulting solid was repeatedly rinsed with anhydrous ethanol followed by deionized water, then dried in a vacuum drying oven at 105 °C for 12 h. Finally, the extracted product was obtained, which was HPC. Each experimental group was conducted in triplicate, and representative samples were selected for characterization.

Table 2. Experimental scheme of samples.

Sample	Solid/g		Liquid/mL	Temperature/°C
	FGZ	Biomass	NMP	
H1 (FGZ/biomass = 100/0)	30	0	1500	350
H2 (FGZ/biomass = 85/15)	25.5	4.5		
H3 (FGZ/biomass = 75/25)	22.5	7.5		
H4 (FGZ/biomass = 65/35)	19.5	10.5		
H5 (FGZ/biomass = 55/45)	16.5	13.5		

The calculation formula of HPC extraction yield is (1):

$$Y\ (\text{wt.\%}) = \frac{m_2}{m_1 \times (1 - A_{ad})} \times 100\% \quad (1)$$

Y: extraction yield; m_1: initial mass of the dry coal sample, g; m_2: mass of the obtained extract, g; A_{ad}: ash content in raw coal, %.

2.3. Characterization of the Extracts

The raw coal and its extraction products were characterized by FTIR (Thermo Fisher Nicolet iS20, Waltham, MA, USA), XPS (Thermo Fisher Nexsa, Waltham, MA, USA), Raman

(Horiba LabRAM HR Evolution, Kyoto, Japan) and XRD (Rigaku SmartLab SE, Tokyo, Japan). XPS and FTIR were used to study the chemical forms and functional groups of raw coal and corresponding extraction products. FTIR was collected in the range of 4000–400 cm^{-1}, with samples prepared via the KBr pellet method. The XPS test adopted Al Kα as the X-ray source. Raman is excited by a 532 nm laser with a spectral scanning range of 800–1800 cm^{-1}. XRD was performed using a Cu target with a scanning speed of 2°/min and a scanning angle range of 10–80°.

2.4. Parameter Fitting Method

All spectral data were processed using standard fitting procedures to extract quantitative parameters. Raman spectra were fitted within the range of 800–1800 cm^{-1} using four Voigt peaks (D1, D2, D3, and G bands) following fluorescent background removal. The I_D/I_G ratio was calculated from the fitted areas of the D1 (~1350 cm^{-1}) and G (~1580 cm^{-1}) bands. XRD patterns were subjected to background correction. The (002) diffraction region was fitted with a combination of Gaussian (γ-band) and Pseudo-Voigt ((002) peak) profiles. The interlayer spacing (d_{002}) and average crystallite stacking height (L_c) were calculated using Bragg's law and the Scherrer equation, respectively. XPS spectra were calibrated against the adventitious carbon C 1s peak at 284.6 eV. High-resolution C 1s and O 1s spectra were fitted with Gaussian–Lorentzian peaks following Shirley background subtraction. The relative atomic percentages of functional groups were determined from the fitted peak areas using standard sensitivity factors.

3. Results and Discussion

3.1. Sample Characterization

3.1.1. Extraction Yield Analysis

Figure 1 illustrates the variations in extraction yield and ash content of the obtained products with varying biomass addition ratios. For this type of coal, as the biomass addition ratio increased from 0% to 35%, the extraction yield rose gradually, peaking at 69.47% when the biomass addition ratio was 35%. This value was approximately 28.32% higher than that of the pure coal group (FGZ raw coal). However, when the biomass proportion was further increased to 45%, the extraction yield decreased markedly to 58.44%. The initial increase in extraction yield is attributable to the synergistic dissolution of active biomass components (e.g., lignin and cellulose) with N-methyl-2-pyrrolidone (NMP), which promotes the depolymerization and dissolution of macromolecular structures in coal, thereby enhancing coal extraction efficiency [15]. The highest extraction yield was achieved at a 35% biomass addition ratio, indicating that the optimal synergistic effect is attained at this ratio. When the biomass addition ratio exceeds 35%, the extraction yield declines significantly, likely due to the increased viscosity of the system and reduced mass transfer efficiency, which weakens the effective interaction between the solvent and coal [27]. Nevertheless, even at higher biomass addition ratios, the extraction yield remains higher than that of the pure FGZ raw coal group without biomass addition.

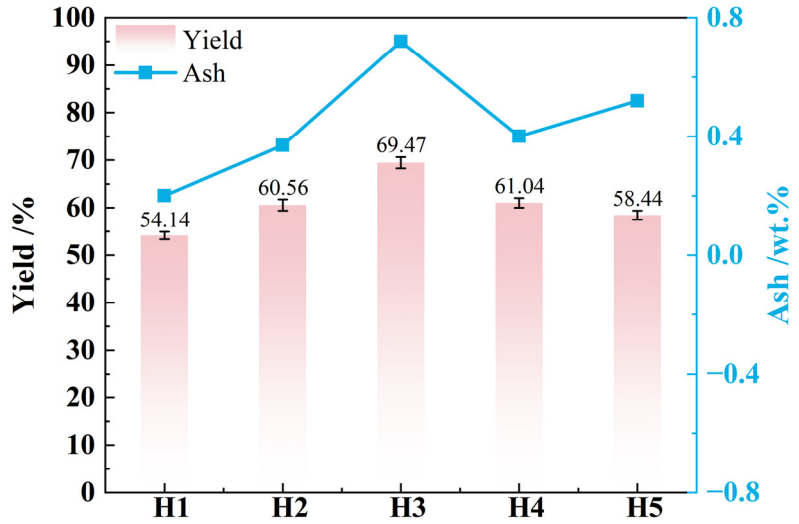


Figure 1. Effects of different biomass additions on extraction yield and ash content.

3.1.2. Proximate and Ultimate Analysis

The results of industrial analysis and elemental analysis of HPC prepared with different biomass addition ratios are presented in Table 3. First, combined with Figure 1, it can be found that both biomass and FGZ raw coal have high ash content. The ash content of all ultra-clean coal is less than 1%, which is significantly lower than that of the raw materials (9.99%). This is attributed to the fact that ash is mainly composed of minerals, which are insoluble in NMP organic solvent. Consequently, the insoluble ash is retained in the residue, thereby reducing the ash content of the final coal product. Secondly, compared with raw coal, the volatile matter content, carbon content, and H/C ratio of HPC are significantly increased, while the fixed carbon content is decreased. With the increase in biomass addition ratio, the volatile matter content gradually increases, indicating that as the proportion of biomass increases, a large amount of hydrogen-rich aliphatic hydrocarbons is solubilized, thereby improving the extraction yield [28]. However, when the biomass addition ratio reaches 45%, the volatile matter content decreases to a certain extent. This may be due to the fact that at a high biomass addition ratio, the solubility of NMP for certain high-volatile-matter components decreases, causing them to be partially retained in the residue rather than entering the HPC product [29]. In general, biomass exhibits a favorable synergistic effect on the extraction of FGZ coal.

Table 3. Proximate and ultimate analysis of samples.

Sample	Proximate Analysis (db, wt.%)			Ultimate Analysis (daf, wt.%)					H/C
	A	V	FC	C	H	O	N	S	
H1	0.20	43.68	54.53	81.62	5.52	7.89	3.11	0.52	0.81
H2	0.37	40.90	57.71	80.67	5.28	8.09	3.15	0.48	0.79
H3	0.72	44.52	52.75	78.63	5.47	9.07	3.94	0.57	0.84
H4	0.40	49.53	47.33	77.22	5.57	10.21	4.34	0.31	0.87
H5	0.52	42.52	56.17	81.03	5.37	8.17	2.85	0.64	0.80

A: ash; V: volatile matter; FC: fixed carbon; db: dry basis; daf: dry ash-free.

3.1.3. SEM Analysis

Figure 2 presents the microstructural morphology of FGZ raw coal and HPC prepared with different biomass addition ratios. It can be observed that FGZ raw coal exhibits a dense lumpy structure with a rough surface, accompanied by a large number of mineral impurity particles. The particle size distribution of FGZ raw coal is uneven, with both large

and fine particles coexisting. Although some impurity particles remain on the surface of HPC, its surface becomes noticeably smoother compared to raw coal and exhibits a small number of pores, with relatively uniform particle dimensions. This indicates that NMP can dissolve small-molecule organic compounds and certain impurities in coal, disrupting its dense structure and rendering the surface smoother and flatter, thereby significantly improving the coal's surface structure. The addition of biomass can further promote this structural modification effect.

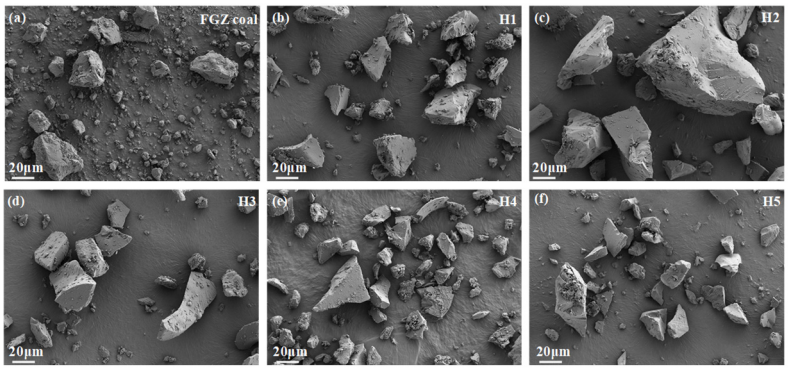


Figure 2. Microstructure of FGZ coal and HPC prepared with different biomass loading levels: (**a**) FGZ coal; (**b**–**f**) H1–H5.

3.1.4. FTIR Analysis

FTIR analysis was performed on raw coal, and the extracts of different biomass addition ratios and the results are presented in Figure 3. It can be observed that the characteristic peaks of the extracted products at 500–600 cm^{-1}, 1000–1100 cm^{-1}, and 3600–3700 cm^{-1} (corresponding to ash) have basically disappeared, with the main characteristic peaks appearing at approximately 1440 cm^{-1}, 1660 cm^{-1}, 2920 cm^{-1}, and 3430 cm^{-1} [30,31]. This indicates that after the synergistic extraction with organic solvent and biomass, the ash content of the extracted products is significantly reduced, while organic components—such as aliphatic hydrocarbons, carbon-oxygen functional groups (C-O and C=O), and hydroxyl groups (-OH)—are effectively retained [15]. This is attributed to the fact that during the thermal extraction process, NMP can dissolve the organic components in raw coal, which in turn enables the effective separation of ash. This result is consistent with the industrial analysis data.

With the increase in biomass addition ratio, the overall intensity of the characteristic peaks of the extracted products basically exhibits a trend of first increasing and then decreasing. When the biomass addition ratio is 15%, the contents of aliphatic hydrocarbons and oxygen-containing functional groups (C=O, -OH) in the extracted products reach the maximum. This suggests that under this ratio, the maximum number of small-molecule compounds in biomass are dissolved, and the hydroxyl groups in both biomass and pulverized coal are solubilized in NMP, thereby increasing the contents of aliphatic hydrocarbons and oxygen-containing functional groups. With a further increase in biomass addition ratio, this may lead to supersaturation of the solvent system or competitive reactions between coal and biomass, resulting in a decrease in the contents of aliphatic hydrocarbons and oxygen-containing functional groups. However, their total contents remain higher than those of the products obtained without biomass addition.

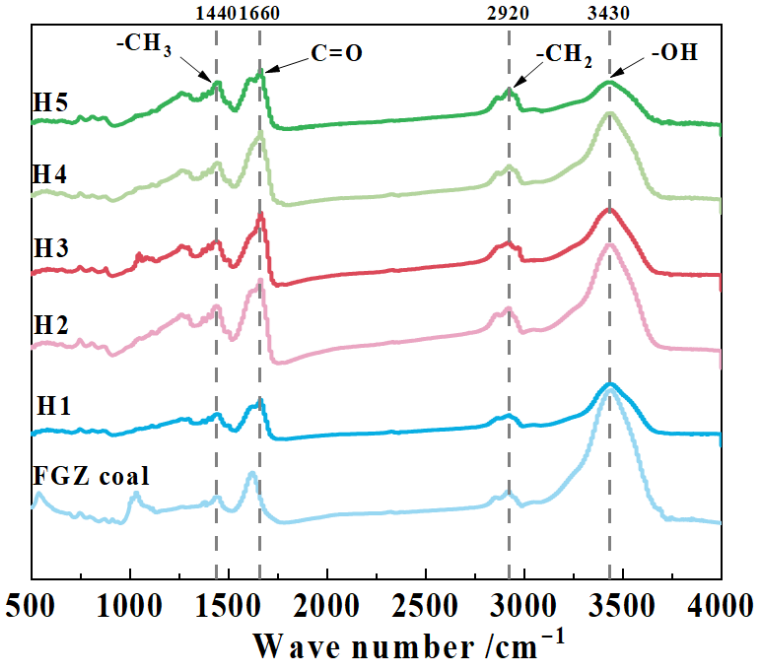


Figure 3. FTIR spectra of HPC prepared with different biomass additions.

3.1.5. Raman Analysis

Raman spectroscopic analysis was conducted on raw coal, and HPC prepared with different biomass addition ratios, and the results are presented in Figure 4a. All samples exhibit distinct characteristic peaks at approximately 1350 cm^{-1} (D peak, corresponding to defect or disordered structures) and 1580 cm^{-1} (G peak, corresponding to the vibration of ideal graphite lattices), which is consistent with the literature [32]. The intensity ratio of the D peak to the G peak (I_D/I_G) is commonly used to evaluate the structural order and defect density of carbon materials; a lower value indicates higher structural order and fewer defects [33]. Figure 4b illustrates the variation in I_D/I_G values among different materials. Gaussian fitting was performed on the spectra in the range of 800–2000 cm^{-1}, resolving four sub-peaks: D1 (~1350 cm^{-1}), D2 (~1200 cm^{-1}), D3 (~1500 cm^{-1}), and G (~1580 cm^{-1}) (Figure 4c–f). These sub-peaks correspond to the vibration modes of six-membered rings, five-membered rings, seven-membered rings, and the ideal graphite crystal structure of carbon materials, respectively [34,35].

The I_D/I_G value of raw coal was 0.8662. As the biomass addition ratio increased from 0% to 45%, the I_D/I_G values of the extracted products were 0.8606, 0.8368, 0.8354, 0.8370, and 0.8416, respectively, showing a trend of first decreasing and then slightly increasing. At a biomass addition ratio of 35%, the I_D/I_G value reached the minimum (0.8354), indicating the highest structural order of HPC. It is observed that the variation trend of the I_D/I_G value of the extracted products is consistent with that of the extraction yield. Notably, the I_D/I_G values of all samples obtained via co-extraction of raw coal and biomass were lower than those of the samples extracted from raw coal alone, indicating that biomass co-extraction promotes the ordered arrangement of the carbon structure during the extraction process. These results are consistent with the FTIR analysis results.

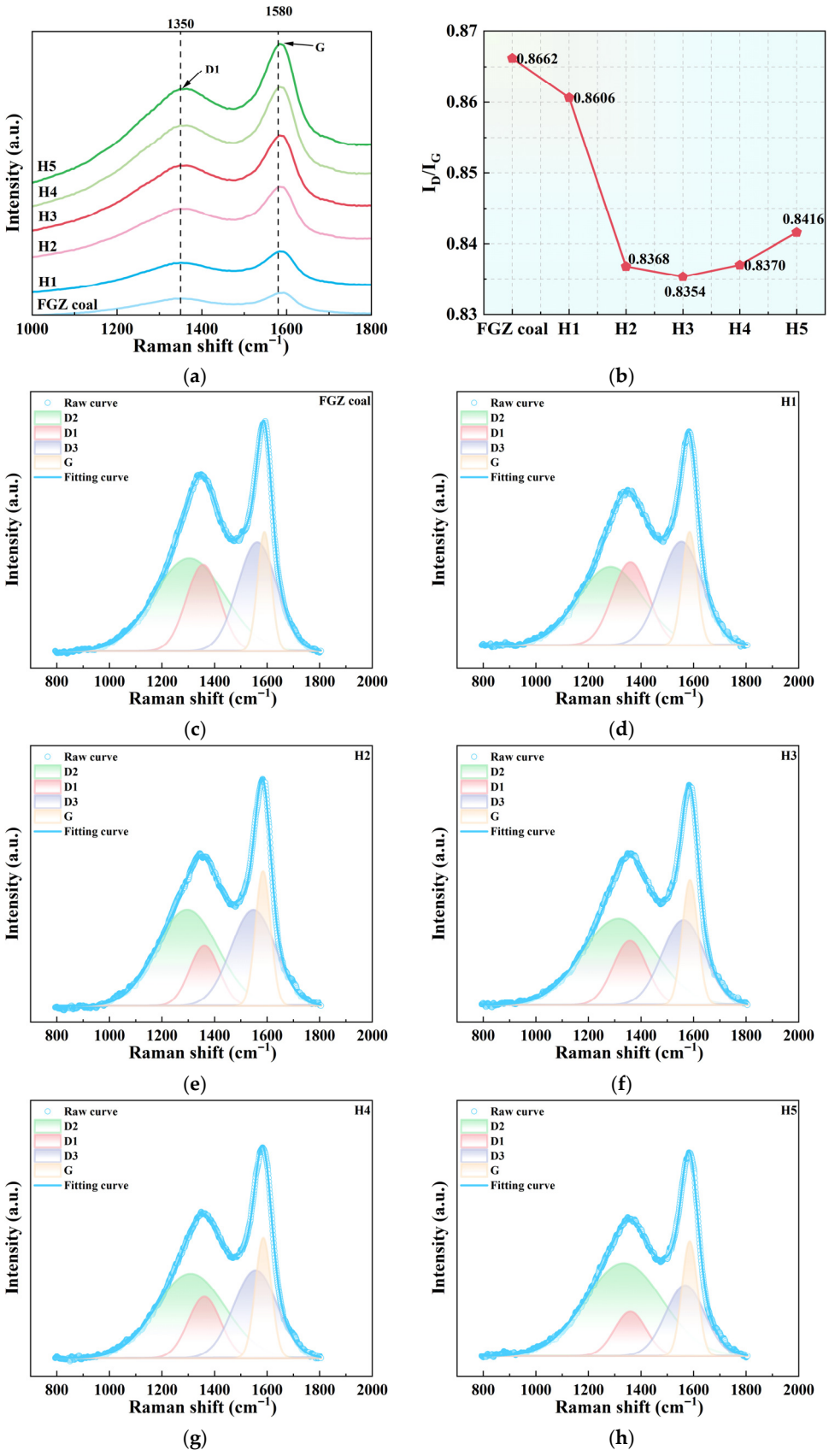


Figure 4. Raman spectra (**a**), I_D/I_G values (**b**) and fitting results (**c**–**h**) of HPC prepared with different biomass additions.

3.1.6. XRD Analysis

XRD analysis was performed on raw coal, and HPC prepared with different biomass addition ratios. The results are presented in Figure 5. As illustrated in the figure, the raw coal exhibits numerous miscellaneous peaks, whereas the extracted products (HPC) display distinct characteristic peaks (γ peak and (002) peak) at 2θ angles of approximately 20° and 25°, with the (100) peak being indistinct [36]. This indicates that a substantial number of aliphatic hydrocarbons are extracted into HPC, which is consistent with the FTIR results. Gaussian fitting was performed on the γ peak and (002) peak of raw coal and HPC, and the microcrystalline layer spacing d_{002} and the microcrystalline stacking height L_c were calculated using the Scherrer Equation [37]. The calculation results are presented in Table 4. The d_{002} value of raw coal is 0.3696 nm, while the d_{002} values of all HPC samples range from 0.3599 nm to 0.3665 nm. In comparison with graphite (0.336–0.337 nm) [38], both raw coal and HPC exhibit a low degree of microcrystalline order; however, the prepared HPC possesses a higher microcrystalline order than raw coal. With the increase in biomass addition ratio, the d_{002} value of the extracted product first decreases and then increases gradually, reaching a minimum when the biomass addition ratio is 25%. This indicates that at a biomass addition ratio of 25%, the aromatic layers of the synergistically extracted product are stacked more closely and regularly, which is consistent with the results from Raman spectroscopy and FTIR analysis. The L_c value can reflect the three-dimensional order of the material [38]. Generally, a higher L_c value corresponds to a greater average stacking height of aromatic layers and a higher structural order of coal. The L_c value of raw coal is 1.5099 nm, and the L_c values of HPC samples range from 1.7133 nm to 2.0569 nm, indicating that HPC has a higher degree of carbon layer stacking and improved structural order compared to raw coal. With the increase in biomass addition ratio, the L_c values of HPC first increase and then decrease, reaching a maximum of 2.0569 nm when the biomass addition ratio is 35%. This demonstrates that at a biomass addition ratio of 35%, the extracted product exhibits the largest crystallite size and the most ordered carbon structure among the prepared samples.

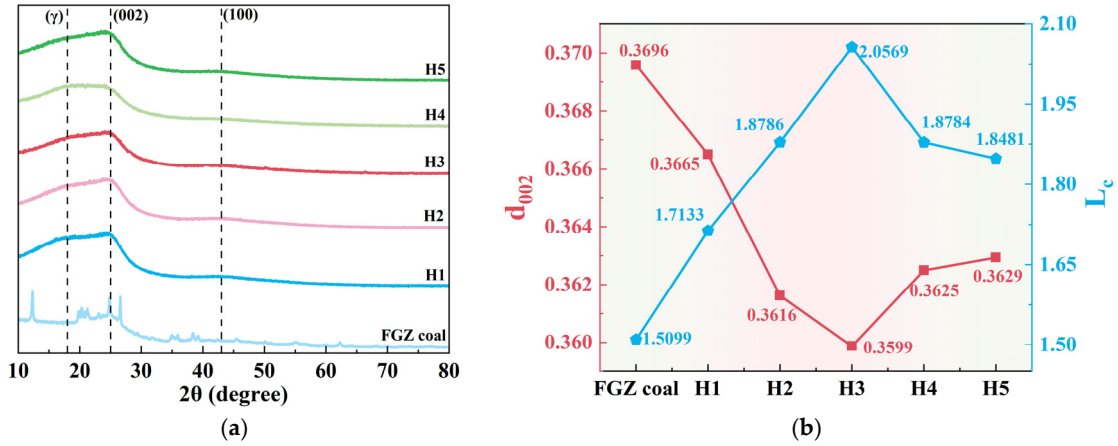


Figure 5. *Cont.*

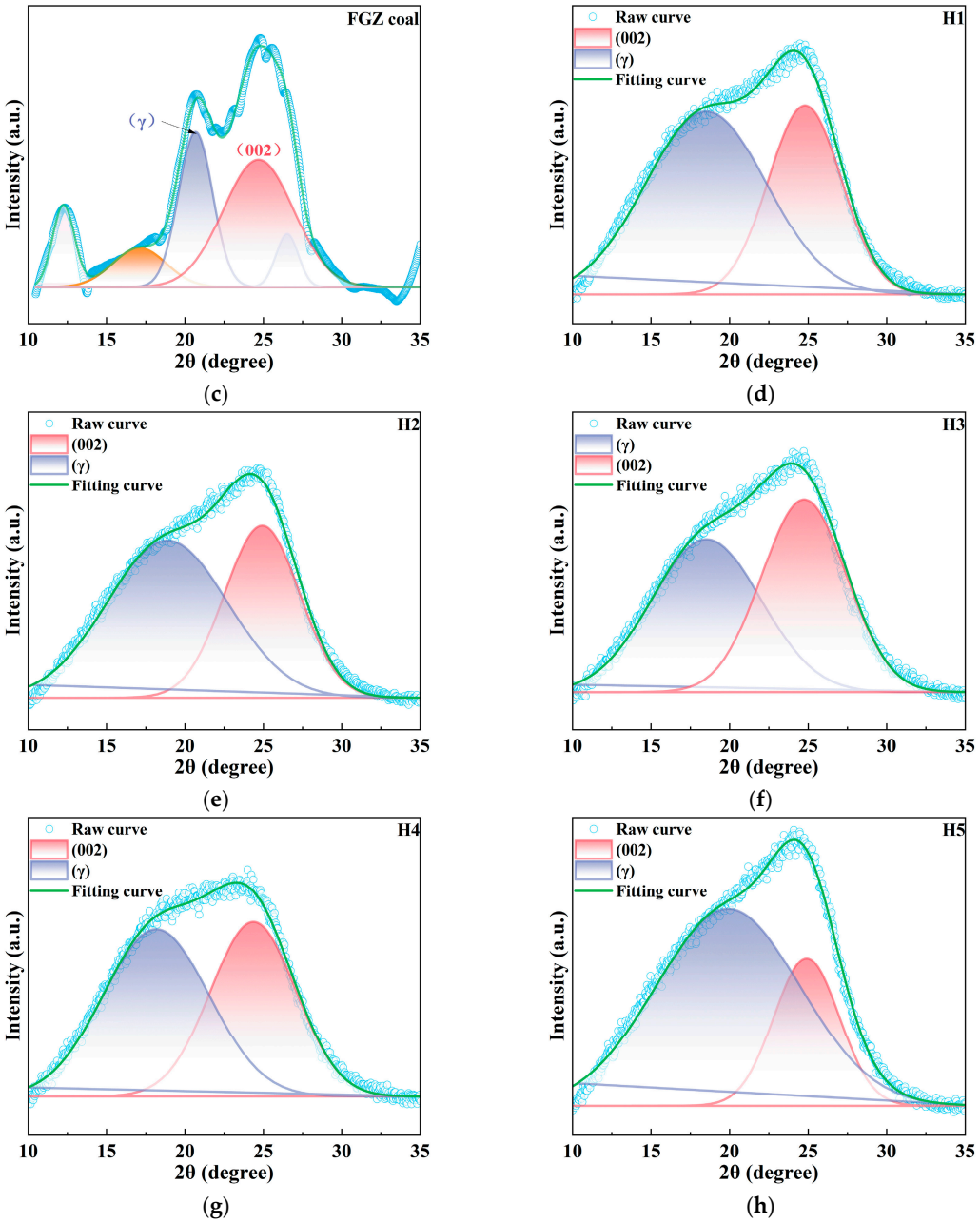


Figure 5. The XRD patterns (**a**) and fitting results (**b**–**h**) of the extracted products prepared with different biomass additions.

Table 4. The microcrystalline structure parameters of the samples.

Sample	2θ(002)/°	FWHM/°	Half-Angle/°	d002/nm	Lc/nm
FGZ coal	24.0642	5.32	12.0321	0.3696	1.5099
H1	24.2658	4.69	12.1329	0.3665	1.7133
H2	24.5982	4.28	12.2991	0.3616	1.8786
H3	24.7191	3.91	12.3596	0.3599	2.0569
H4	24.5378	4.23	12.2689	0.3625	1.9006
H5	24.5076	4.35	12.2538	0.3629	1.8481

3.1.7. XPS Analysis

XPS analysis was employed to investigate the existing forms of C (C1s) and O (O1s) elements in HPC prepared with different biomass additions, followed by peak fitting. The XPS results are presented in Figure 6. Deconvolution results of the C 1s and O 1s spectra

indicate that the C 1s peak can be deconvoluted into four sub-peaks, corresponding to C-C (~284.6 eV), C-O (~286 eV), C=O (~287.6 eV), and COO^- (~288.9 eV) [15]. It can be observed that the C element exists primarily in three forms, with the proportion of C-C (an indicator of structural order) being significant (>75%). Raw coal exhibited the lowest C-C ratio (77.24%), while HPC consistently demonstrated values exceeding 80%. With the increase in biomass addition ratio, the peak intensity of the C-C peak first increased and then slightly decreased, indicating that the structural order of the extracted product also first increased and then slightly decreased. This is consistent with the results obtained from Raman spectroscopy and X-ray diffraction (XRD) analysis. The O 1s peak can also be deconvoluted into four sub-peaks, corresponding to C=O (~532 eV), C-OH (~532.7 eV), C-O- (~533.4 eV), and COOH (~534.3 eV) [15]. Similarly, the O element exists primarily in three forms, with C=O accounting for a significant proportion among all oxygen-containing functional groups (>55%). Raw coal exhibits the lowest C=O ratio (57.08%), while HPC consistently demonstrates values exceeding 60%. With the increase in biomass addition ratio, the content of C=O in the extracted product first increased and then slowly decreased, indicating a reduction in the number of oxygen-containing functional groups on the surface of the extracted product, thereby decreasing surface defects. This result is also consistent with those from Raman spectroscopy and XRD analysis.

3.2. Extraction Mechanism

When NMP solvent was employed for extraction at 350 °C, different biomass addition ratios exerted a significant influence on the synergistic preparation mechanism of HPC. The mechanism diagram of the extraction process is shown in Figure 7. During the concurrent pyrolysis and solvent interaction of coal and biomass, lignin and cellulose in biomass underwent pyrolysis initially, generating active functional groups such as phenoxy groups. Subsequently, coal initiated pyrolysis, releasing aliphatic hydrocarbons, carboxylic acid compounds, and partial aromatic fragments. Through the formation of hydrogen bond interactions (Ar-O-OH-R and π-OH-R), a complex soluble in NMP was formed. Consequently, with the increase in biomass addition ratio, certain carboxylic acids and aliphatic hydrocarbons were solubilized, which reduced the stability of the cross-linked macromolecular network structure in coal, enhanced the penetration and swelling capacity of NMP into coal particles, and enabled more NMP molecules to penetrate the spatial network structure of coal, thereby improving the extraction yield. However, with the further increase in biomass addition, excessive phenoxy groups are generated, which then undergo self-condensation reactions, and stable ether bond structures such as diphenyl ether (Ar-O-Ar) are formed. This thus weakened the penetration and swelling capacity of NMP into coal particles. Meanwhile, excessive biomass residues and intermediate products may increase the system viscosity, hindering the diffusion of NMP molecules and thereby reducing the extraction yield. This mechanism is consistent with the evolution of functional groups, changes in structural order, and variations in surface chemical states revealed by FTIR, Raman and XPS. It adequately explains the phenomenon observed in this study that the extraction yields first increases and then decreases with the increase in biomass addition ratio. It is worth noting that in the current stage of this research, direct experimental verification of specific intermediate species has not yet been conducted. Future studies should employ more direct analytical techniques to track the formation and transformation of key intermediates during the co-extraction process.

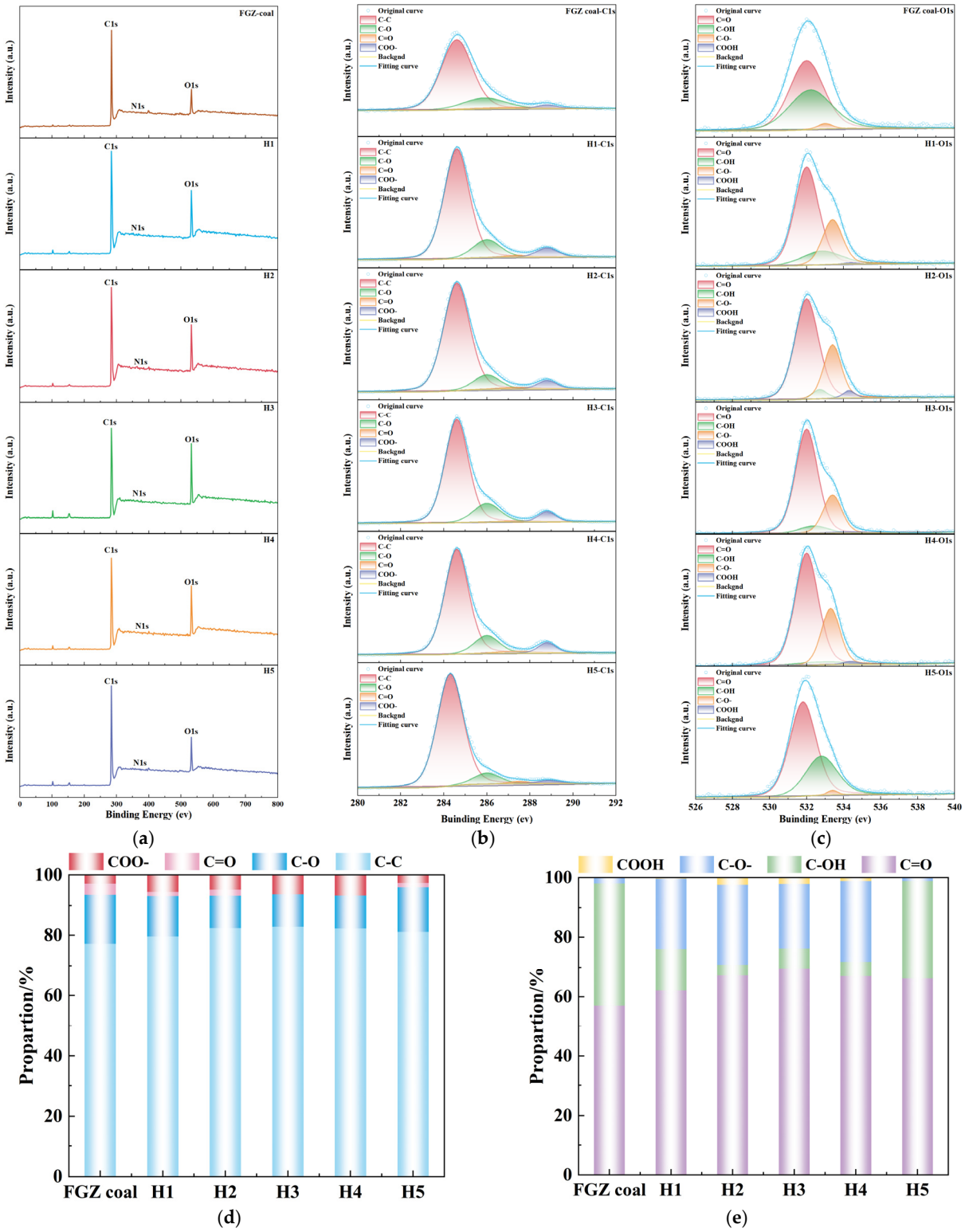


Figure 6. XPS analysis results: XPS full spectrum (**a**), C spectrum fitting results (**b**), O spectrum fitting results (**c**), C element existence form proportion (**d**) and O element existence form proportion (**e**) of HPC.

https://doi.org/10.3390/pr14030404

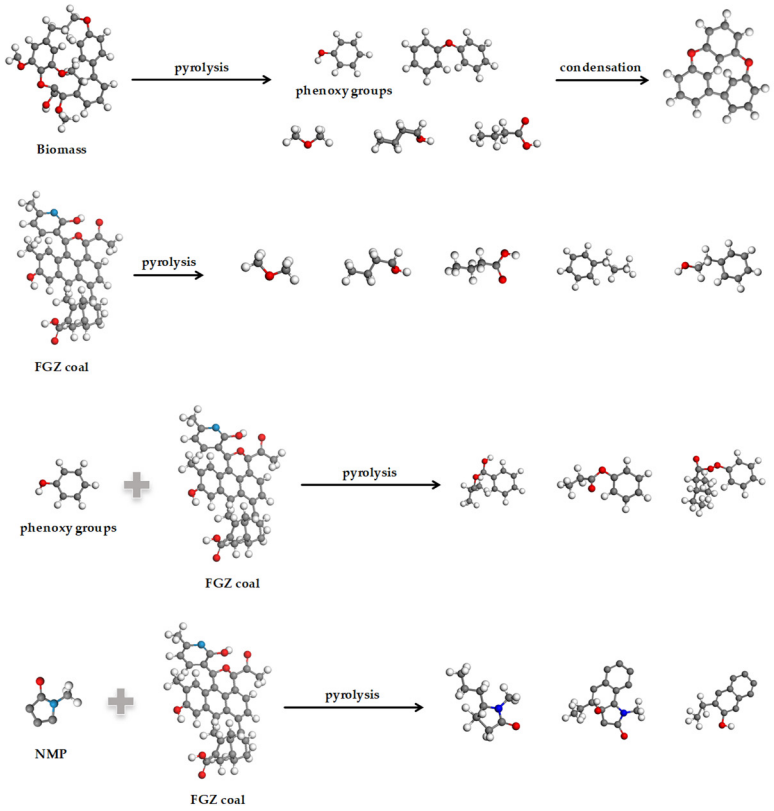


Figure 7. Mechanism diagram of the extraction process (Gray, white, red, blue, and yellow represent C, H, O, N, and S, respectively.).

3.3. Application Industries

The high-performance carbon (HPC) prepared in this study exhibits characteristics of low ash content, high volatile matter content, and improved carbon structural order, thus possessing broad application prospects in the materials, metallurgy, and energy industries. It constitutes one of the important approaches to achieving efficient, clean, and high-value utilization of coal resources.

In the materials field, HPC serves as an ideal precursor for preparing high-performance carbon materials. Its high aromatic content and excellent plasticity facilitate the production of low-cost carbon fibers [39]. Meanwhile, its low ash content and high carbon content enable it to be used in manufacturing high-specific-surface-area activated carbon for supercapacitor electrodes [40]. In the metallurgical field, HPC contributes to alleviating the shortage of high-quality coking coal [41]. Incorporating HPC into conventional coking processes allows for the addition of more weakly caking coal while ensuring coke quality, thereby reducing production costs. In the hot-pressing process, HPC can also act as a hot-briquetting binder to produce high-strength briquettes [42,43], further reducing dependence on scarce coking coal. This is of great significance for ensuring raw material security and promoting the green transformation of the iron and steel industry. In the field of energy conversion, HPC can be directly used as an ideal fuel for direct carbon fuel cells (DCFCs) and chemical looping combustion (CLC) systems, realizing efficient and clean coal-fired power generation as well as near-zero carbon dioxide emissions [44].

Although the preparation process of HPC involves organic solvents and biomass additives, presenting certain complexities and energy consumption, its significant advantages in ash removal (>90%), enhanced structural order, and role as a precursor for high-performance carbon materials make high-value utilization feasible. Future research should focus on process integration and efficient solvent recovery to further reduce produc-

tion costs. Preliminary assessments indicate that when HPC is applied in high-end markets such as carbon fiber or supercapacitor electrodes, its economic viability significantly outperforms traditional coal utilization pathways.

4. Conclusions

In this study, the synergistic extraction of FGZ coal with biomass was systematically investigated. The main conclusions are as follows:

1. The addition of biomass significantly enhanced the extraction yield of FGZ coal, with an optimum yield of 69.47% achieved at 35% biomass addition—an increase of approximately 28.32% compared to coal-only extraction.
2. Biomass co-extraction effectively reduced the ash content of the resulting HPC to below 1%, demonstrating efficient mineral separation during the solvent extraction process.
3. SEM analysis indicated that the dense, lumpy structure with rough surface and adhered mineral impurities in raw FGZ coal was effectively modified after treatment. The resulting HPC exhibited a smoother surface, and a more uniform particle size.
4. Raman and XRD analyses revealed that biomass addition promoted structural ordering in the extracted products, with the lowest I_D/I_G ratio (0.8345) and the highest microcrystalline stacking height (L_c = 2.0569 nm) observed at 35% biomass addition.
5. FTIR and XPS analyses confirmed the retention of aliphatic and oxygen-containing functional groups in the extracts, supporting the proposed synergistic mechanism involving hydrogen-bond interactions and solvent penetration enhancement.
6. The findings suggest that biomass-assisted solvothermal extraction is a promising pathway for producing high-quality, low-ash HPC with potential applications in carbon materials, metallurgy, and clean energy systems.

This study primarily investigated the extraction rate, microstructure, structural sequence, and chemical composition of HPC. Subsequent research will comprehensively characterize the physicochemical properties of HPC, including its calorific value and porosity.

Author Contributions: Conceptualization, Y.K.; methodology, H.Z. (Hailan Zhao); software, Y.K.; validation, Y.K.; formal analysis, Y.Y.; investigation, Y.K.; resources, Y.K. and H.Z. (Hailan Zhao); data curation, Y.K.; writing—original draft preparation, Y.K.; writing—review and editing, H.Z. (Hailan Zhao) and H.Z. (Haibin Zuo); visualization, Y.K.; supervision, H.Z. (Haibin Zuo); project administration, H.Z. (Haibin Zuo); funding acquisition, H.Z. (Haibin Zuo). All authors have read and agreed to the published version of the manuscript.

Funding: This research was funded by National Natural Science Foundation of China, grant number (52474345) and Minmetals Science and Technology Special Plan, grant number (2025ZXA05).

Data Availability Statement: The original contributions presented in this study are included in the article. Further inquiries can be directed to the corresponding authors.

Conflicts of Interest: The authors declare no conflicts of interest.

Abbreviations

The following abbreviations are used in this manuscript:

FGZ	Fangezhuang Coal
FTIR	Fourier transform infrared spectroscopy
Raman	Raman spectroscopy
XRD	X-ray diffraction
XPS	X-ray photoelectron spectroscopy

References

1. Chen, J.; Yang, S.; Qian, Y. A novel path for carbon-rich resource utilization with lower emission and higher efficiency: An integrated process of coal gasification and coking to methanol production. *Energy* **2019**, *177*, 304–318. [CrossRef]
2. Li, Z.; Zhu, S.; Ouyang, Z.; Zhu, Z.; Lyu, Q. Progress in Caking Mechanism and Regulation Technologies of Weakly Caking Coal. *Energies* **2025**, *18*, 4178. [CrossRef]
3. Rahman, M.; Samanta, A.; Gupta, R. Production and characterization of ash-free coal from low-rank Canadian coal by solvent extraction. *Fuel Process. Technol.* **2013**, *115*, 88–98. [CrossRef]
4. Chandaliya, V.; Biswas, P.; Dash, P.; Sharma, D. Producing low-ash coal by microwave and ultrasonication pretreatment followed by solvent extraction of coal. *Fuel* **2018**, *212*, 422–430. [CrossRef]
5. Liu, M.; Tao, Y.; Yang, Y.; Lei, Z. Structural Characterization of HyperCoal Extracts from the Depolymerization of Shengli Lignite Using NaOH/Methanol. *Processes* **2025**, *13*, 1821. [CrossRef]
6. Sönmez, Ö.; Yıldız, Ö.; Çakır, M.Ö.; Gözmen, B.; Giray, E.S. Influence of the addition of various ionic liquids on coal extraction with NMP. *Fuel* **2018**, *212*, 12–18. [CrossRef]
7. White, C.; Rohar, P.; Veloski, G.; Anderson, R. Practical notes on the use of N-Methyl-2-pyrrolidinone as a solvent for extraction of coal and coal-related materials. *Energy Fuels* **1997**, *11*, 1105–1106. [CrossRef]
8. Wang, J.; Li, C.; Sakanishi, K.; Nakazato, T.; Tao, H.; Takanohashi, T.; Takarada, T.; Saito, I. Investigation of the remaining major and trace elements in clean coal generated by organic solvent extraction. *Fuel* **2005**, *84*, 1487–1493. [CrossRef]
9. Okuyama, N.; Komatsu, N.; Shigehisa, T.; Kaneko, T.; Tsuruya, S. Hyper-coal process to produce the ash-free coal. *Fuel Process. Technol.* **2004**, *85*, 947–967. [CrossRef]
10. Yang, J.; Nakabayashi, K.; Miyawaki, J.; Yoon, S.-H. Preparation of isotropic pitch-based carbon fiber using hyper coal through co-carbonation with ethylene bottom oil. *J. Ind. Eng. Chem.* **2016**, *34*, 397–404. [CrossRef]
11. Okuma, S.; Moriyasu, Y.; Inoue, T.; Shishido, T.; Hamaguchi, M.; Toyoda, M. Discussion of the factors affecting the Electric double-layer capacitors characteristics of Hyper coal-derived carbon powder. *Carbon Rep.* **2025**, 050103. [CrossRef]
12. Zhao, J.; Mangi, H.N.; Zhang, Z.; Chi, R.a.; Zhang, H.; Xian, M.; Liu, H.; Zuo, H.; Wang, G.; Xu, Z. The structural characteristics and gasification performance of cokes of modified coal extracted from the mixture of low-rank coal and biomass. *Energy* **2022**, *258*, 124864. [CrossRef]
13. Li, X.; Zhu, X.-q.; Okuda, K.; Zhang, Z.; Ashida, R.; Yao, H.; Miura, K. Preparation of carbon fibers from low-molecular-weight compounds obtained from low-rank coal and biomass by solvent extraction. *New Carbon Mater.* **2017**, *32*, 41–47. [CrossRef]
14. Shui, H.; Shan, C.; Cai, Z.; Wang, Z.; Lei, Z.; Ren, S.; Pan, C.; Li, H. Co-liquefaction behavior of a sub-bituminous coal and sawdust. *Energy* **2011**, *36*, 6645–6650. [CrossRef]
15. Zhao, J.; Zuo, H.-b.; Wang, J.-s.; Xue, Q.-g. The mechanism and products for co-thermal extraction of biomass and low-rank coal with NMP. *Int. J. Miner. Metall. Mater.* **2019**, *26*, 1512–1522. [CrossRef]
16. Kang, H.; Wang, J.; Chen, F.; Rong, T.; Yu, Y.; Ding, W.; Zuo, H. Investigation on the mechanism of solvothermal extraction of coals by macromolecular models. *Fuel* **2024**, *355*, 129547. [CrossRef]
17. Han, C.; Wei, G.; Zhu, R.; Li, C.; Wang, R. Biochar-based direct reduced iron production for short-process steelmaking: Current research status and future prospects. *Int. J. Hydrogen Energy* **2025**, *157*, 150524. [CrossRef]
18. Liu, Y.; Zhi, J.; Lyu, Z.; Gu, C.; Diao, W.; Qu, Z.; Bao, Y. Structure and transport behavior of the CaO-SiO_2-Al_2O_3-La_2O_3 system: Insights from molecular dynamics simulations. *Ceram. Int.* **2025**, *51*, 38855–38863. [CrossRef]
19. Fahmy, T.Y.; Fahmy, Y.; Mobarak, F.; El-Sakhawy, M.; Abou-Zeid, R.E. Biomass pyrolysis: Past, present, and future. *Environ. Dev. Sustain.* **2020**, *22*, 17–32. [CrossRef]
20. Fabozzi, A.; Cerciello, F.; Senneca, O. Direct reduction of iron ore using biomass biochar: Reduction rate, microstructural and morphological analysis. *Fuel* **2025**, *383*, 133976. [CrossRef]
21. Coppola, A.; Scala, F. Chemical looping for combustion of solid biomass: A review. *Energy Fuels* **2021**, *35*, 19248–19265. [CrossRef]
22. Periyasamy, M.; Radhakrishnan, L.; Sengupta, U.; Sain, S.; Pichandi, C.; Mukhopadhyay, S.; Kar, A. Phase transformation assisted reduction roasting of low-grade iron ore via industrial biomass as a reductant. *Biomass Convers. Biorefinery* **2025**, *15*, 14603–14617. [CrossRef]
23. Top, S.; Altiner, M.; Kursunoglu, S. Separation of Mn and Fe from a Manganiferous Iron Ore Using Horse Dung as Reductant: A Zero Waste Approach. *JOM* **2022**, *74*, 474–483. [CrossRef]
24. Top, S.; Altiner, M.; Vapur, H.; Kursunoglu, S.; Stopic, S. A Novel Biomass-Derived Reductant for Nitric Acid Dissolution of Manganiferous Iron Ore: Comparative Assessment of Organic Reductants. *Minerals* **2026**, *16*, 47. [CrossRef]
25. *ASTM D3172–13*; Standard Practice for Proximate Analysis of Coal and Coke. ASTM International: West Conshohocken, PA, USA, 2021.
26. *ASTM D3176–15*; Standard Practice for Ultimate Analysis of Coal and Coke. ASTM International: West Conshohocken, PA, USA, 2016.

27. Zhang, J.; Fu, H.; Liu, Y.; Dang, H.; Ye, L.; Conejo, A.N.; Xu, R. Review on biomass metallurgy: Pretreatment technology, metallurgical mechanism and process design. *Int. J. Miner. Metall. Mater.* **2022**, *29*, 1133–1149. [CrossRef]
28. Zhang, J.; Zhang, K.; Huang, J.; Feng, Y.; Yellezuome, D.; Zhao, R.; Chen, T.; Wu, J. Synergistic effect and volatile emission characteristics during co-combustion of biomass and low-rank coal. *Energy* **2024**, *289*, 130015. [CrossRef]
29. Dang, H.; Xu, R.; Zhang, J.; Wang, M.; Ye, L.; Jia, G. Removal of oxygen-containing functional groups during hydrothermal carbonization of biomass: Experimental and DFT study. *Energy* **2023**, *276*, 127436. [CrossRef]
30. Tang, J.; Wang, Z.; Xue, Q.; Wang, G.; Wang, G.; Wang, J. From Sweet Potato Byproducts to Energy Storage: Unveiling the Potential of Foaming Syrup as a High-Performance Hard Carbon Anode for Sodium-Ion Batteries. *ACS Omega* **2025**, *10*, 34266–34275. [CrossRef]
31. Lin, S.; Liu, Z.; Zhao, E.; Qian, J.; Li, X.; Zhang, Q.; Ali, M. A study on the FTIR spectra of pre-and post-explosion coal dust to evaluate the effect of functional groups on dust explosion. *Process Saf. Environ. Prot.* **2019**, *130*, 48–56. [CrossRef]
32. Chen, Z.; Gu, Y.; Hu, L.; Xiao, W.; Mao, X.; Zhu, H.; Wang, D. Synthesis of nanostructured graphite via molten salt reduction of CO_2 and SO_2 at a relatively low temperature. *J. Mater. Chem. A* **2017**, *5*, 20603–20607. [CrossRef]
33. Yu, J.; Guo, Q.; Ding, L.; Gong, Y.; Yu, G. Studying effects of solid structure evolution on gasification reactivity of coal chars by in-situ Raman spectroscopy. *Fuel* **2020**, *270*, 117603. [CrossRef]
34. Moura, T.A.; Neves, W.Q.; Alencar, R.S.; Kim, Y.A.; Endo, M.; Vasconcelos, T.L.; Costa, D.G.; Candiotto, G.; Capaz, R.B.; Araujo, P.T. Resonance Raman spectroscopy characterization of linear carbon chains encapsulated by multi-walled carbon nanotubes. *Carbon* **2023**, *212*, 118123. [CrossRef]
35. Finnie, P.; Ouyang, J.; Fagan, J.A. Broadband full-spectrum Raman excitation mapping reveals intricate optoelectronic–vibrational resonance structure of chirality-pure single-walled carbon nanotubes. *ACS Nano* **2023**, *17*, 7285–7295. [CrossRef]
36. Jiang, J.; Zhang, S.; Longhurst, P.; Yang, W.; Zheng, S. Molecular structure characterization of bituminous coal in Northern China via XRD, Raman and FTIR spectroscopy. *Spectrochim. Acta Part A Mol. Biomol. Spectrosc.* **2021**, *255*, 119724. [CrossRef] [PubMed]
37. Zhang, X.; Zhang, S.; Li, P.; Ding, Z.; Hao, Z. Investigation on solubility of multicomponents from semi-anthracite coal and its effect on coal structure by Fourier transform infrared spectroscopy and X-ray diffraction. *Fuel Process. Technol.* **2018**, *174*, 123–131. [CrossRef]
38. Vanitha, M.; Camellia, P.; Balasubramanian, N. Augmentation of graphite purity from mineral resources and enhancing% graphitization using microwave irradiation: XRD and Raman studies. *Diam. Relat. Mater.* **2018**, *88*, 129–136. [CrossRef]
39. Yang, J.; Nakabayashi, K.; Miyawaki, J.; Yoon, S.-H. Preparation of pitch based carbon fibers using Hyper-coal as a raw material. *Carbon* **2016**, *106*, 28–36. [CrossRef]
40. Liu, Y.; Cao, W.-D.; Fan, X.; Hou, R.-R.; Bai, X.; Zhang, X.-Y.; Li, Y.; Zhao, G.-M.; Liang, P. Porous carbon prepared by thermal dissolution of coal and biomass for high-performance supercapacitors. *Fuel* **2024**, *369*, 131677. [CrossRef]
41. Zhao, J.; Zuo, H.; Wang, G.; Wang, J.; Xue, Q. Improving the coke property through adding HPC extracted from the mixture of low-rank coal and biomass. *Energy Fuels* **2019**, *34*, 1802–1810. [CrossRef]
42. Wang, Y.; Zuo, H.; Bai, K.; Zhao, J.; Chen, J. Characterization of the Hot-Pressed Coal Briquettes Prepared with the HyperCoal. In *Energy Technology 2020: Recycling, Carbon Dioxide Management, and Other Technologies*; Springer: Berlin/Heidelberg, Germany, 2020; pp. 57–67. [CrossRef]
43. Yu, Y.; Zuo, H.; Wang, Y.; Kang, H.; Guo, H.; Rong, T.; Wang, J. Thermal extraction of coal and derivatives to prepare hot-pressed coal briquette for COREX application. *Fuel* **2024**, *357*, 129773. [CrossRef]
44. Dudek, M.; Tomczyk, P.; Socha, R.; Hamaguchi, M. Use of ash-free "Hyper-coal" as a fuel for a direct carbon fuel cell with solid oxide electrolyte. *Int. J. Hydrogen Energy* **2014**, *39*, 12386–12394. [CrossRef]

Disclaimer/Publisher's Note: The statements, opinions and data contained in all publications are solely those of the individual author(s) and contributor(s) and not of MDPI and/or the editor(s). MDPI and/or the editor(s) disclaim responsibility for any injury to people or property resulting from any ideas, methods, instructions or products referred to in the content.